

# Gravitational perturbations of Schwarzschild spacetime at null infinity and the hyperboloidal initial value problem

Anil Zenginoğlu<sup>1,2,3</sup>, Darío Núñez<sup>3,4</sup>, Sascha Husa<sup>3,5</sup>

<sup>1</sup> *Department of Physics, University of Maryland, College Park, MD 20742, USA*

<sup>2</sup> *Center for Scientific Computation and Mathematical Modeling,  
University of Maryland, College Park, MD 20742, USA*

<sup>3</sup> *Max-Planck-Institut für Gravitationsphysik, Albert-Einstein-Institut, 14476 Golm, Germany*

<sup>4</sup> *Instituto de Ciencias Nucleares, Universidad Nacional Autónoma de México, A.P. 70-543, México D.F. 04510, México, and*

<sup>5</sup> *Departament de Física, Universitat de les Illes Balears,  
Cra. Valldemossa Km. 7.5, E-07122 Palma de Mallorca, Spain*

We study gravitational perturbations of Schwarzschild spacetime by solving a hyperboloidal initial value problem for the Bardeen-Press equation. Compactification along hyperboloidal surfaces in a scri-fixing gauge allows us to have access to the gravitational waveform at null infinity in a general setup. We argue that this hyperboloidal approach leads to a more accurate and efficient calculation of the radiation signal than the common approach where a timelike outer boundary is introduced. The method can easily be generalized to study perturbations of Kerr spacetime using the Teukolsky equation.

PACS numbers: 04.25.Nx, 04.25.Dg, 04.20.Ha

## I. INTRODUCTION

In the last few years, numerical relativity has made tremendous progress in treating the inspiral of compact objects, starting with the breakthrough simulations of [1–3]. Rather accurate simulations of the last  $\approx 10$  orbits of roughly equal mass binary black holes have become standard in the field (see e.g. [4–8] for recent examples). However, these simulations are still restricted to finite outer boundaries and gravitational radiation is extracted at a number of finite shells. Maybe not surprisingly, it has been found that the wave extraction radius is a significant limiting factor for the precision of results [9, 10]. The practical implementation of algorithms that include null infinity in the numerical grid is thus highly desirable. It also provides for a fruitful problem to foster the interaction of numerical and mathematical relativity.

An important stepping stone to develop such algorithms is the case of linearized perturbations on a fixed background. The numerical study of linearized perturbations is convenient as one can evolve the gravitational radiation very accurately for a comparatively low computational cost [11–13]. For evolutions along null surfaces this has provided important guidance in the past, see e.g. [14–16]. Note, however, that linear analysis may not be valid in certain special weak field situations. Examples where the linear analysis breaks down have been found in studies of test fields [17, 18]. In the pure gravitational case, so far it seems that the perturbative analysis fits well with the nonlinear evolution [12, 19–22].

When the background spacetime describes the particularly interesting case of a (stationary) black hole, the perturbation equations take the form of linear wave equations with a potential term (in our case the Bardeen-Press equation [23]). The solutions to such equations show three stages: an initial transient (the “direct signal”), quasi-normal mode ringing and power-law decay. The standard method to numerically analyze these stages in the time domain has been to solve initial boundary value problems using Cauchy-type foliations. This method has certain disadvantages. When one is primarily interested in radiative properties of the solution far away from the source, the use of Cauchy-type foliations is a waste of computational resources. Furthermore, there are difficulties related to the choice of boundary conditions. It has been shown that a typical choice of boundary data for numerical relativity destroys the polynomial tail behavior of solutions to wave equations on a Schwarzschild spacetime [24, 25]. Note that even if the polynomial tail can be calculated by using a better choice of boundary data, the decay rate will be the one near time-like infinity. It has been pointed out, however, that the relevant decay rate for an astrophysical observer is the one along null infinity [26–28].

Using foliations that approach null infinity would cure these problems. Numerical studies of gravitational perturbations at null infinity have been performed by [14, 15] using a characteristic approach for the Bardeen-Press equation, and have been compared with fully nonlinear studies in [16]. The authors have been able to efficiently calculate the quasi-normal mode ringing and the power law decay. There are, however, two main difficulties in the characteristic approach. An important aspect of solving the Bardeen-Press equation instead of the Regge-Wheeler-Zerilli equations is that the favorable separability properties of the Teukolsky formalism extends to Kerr spacetime [29]. Unfortunately, generalizing the studies of [14, 15] to Kerr spacetime is complicated because the construction of

null foliations smoothly covering Kerr spacetime is not straightforward and from a numerical point of view not very convenient [30, 31]. A further complication is related to the causal structure of a black hole spacetime. Due to the global relationship between null surfaces on which boundary information is known to pose a characteristic initial value problem, the numerical solution for a perturbed black hole needs to be calculated in two steps: advanced [15] and retarded [14]. A related difficulty shows itself also in the choice of suitable coordinates which allow the computation of the gravitational waveform at null infinity and provide good resolution near the horizon.

An alternative, and very flexible approach to study radiation at null infinity is to use spacelike surfaces. Following [32] we call such surfaces hyperboloidal and the related initial value problem a hyperboloidal initial value problem. Hyperboloidal surfaces are as flexible as Cauchy-type surfaces because the property that characterizes them is not local but global. Further, they enable, like characteristic surfaces, a clean treatment of gravitational radiation because they approach null infinity. In this sense, they are hoped to combine the “best of both worlds”, and we expect increasing interest in this approach.

In the present paper we want to learn from the linearized case as a preparation for the nonlinear hyperboloidal initial value problem. To this end we construct solutions of the Bardeen-Press equation by numerically solving a hyperboloidal initial value problem for the perturbations of Schwarzschild spacetime and we calculate the gravitational wave signal at null infinity. We find that compactification along hyperboloidal surfaces leads to a very efficient code. Specifically, we show that the calculation of the quasi-normal mode frequencies in the time domain can be performed accurately with a small number of grid points using standard numerical techniques. The last stage of the solution, namely the power-law decay, can be numerically calculated if the resolution is sufficiently high. A major advantage of our method for this part of the signal is not so much the efficiency but rather the fact that we can measure the decay rate at null infinity by solving a Cauchy problem in the PDE sense.

In the presentation and, to some extent, in the choice of the methods applied in the paper, we tried to avoid a heavy use of the conformal language. Our philosophy of constructing an algorithm for the hyperboloidal initial value problem follows the suggestion in [33]. Instead of constructing a gauge-independent, regular, conformal Bardeen-Press equation, we make a suitable use of our gauge freedom before compactifying the coordinates and show that, in the end, regular equations are obtained. While both approaches are equivalent in their final aim, we hope that the way we present the method will be more accessible to numerical relativists who are not familiar with notions related to conformal geometry.

The paper is organized as follows: In section II we present the Teukolsky formalism and derive the Bardeen-Press equation for a spherically symmetric but otherwise arbitrary foliation. In the third section we discuss our method to include null infinity on a numerical grid. We show that the hyperboloidal Bardeen-Press equation written in compactifying coordinates is regular at null infinity. After a short presentation of our numerical methods in section IV, we go over to the numerical studies of the last two stages for the gravitational perturbations where we demonstrate some of the basic advantages of the hyperboloidal approach in numerical work. In the discussion section we summarize our results and point out some ideas for future work.

## II. THE PERTURBATION EQUATION

### 1. General definitions

Teukolsky [29] derived a master perturbation equation for various fields in a Kerr background, using the spinor formalism introduced by Newman and Penrose [34]. One of the central ideas of this formulation consists in choosing a tetrad of null vectors,  $Z_a{}^\mu$ , and then defining the directional operators as the projections of the covariant derivative along each null vector. For a complete review on the subject and its properties, the reader is referred to [35, 36].

Usually the tetrad is defined with four null vectors, two real and along the light cone and the other two complex conjugate and in the perpendicular plane to the cone. It can be seen that there is much room for conventions regarding the orientation and scaling of the null factors, and consequently for confusion. We make the following choice: we label the two real vectors along the light cone as  $Z_0{}^\mu = l^\mu$ ,  $Z_1{}^\mu = k^\mu$  and choose them both future directed and with  $l^\mu$  pointing outward, and  $k^\mu$  pointing inward. The other two null vectors, in the perpendicular plane, will be denoted by a complex vector,  $m^\mu$ :  $Z_2{}^\mu = m^\mu$ ,  $Z_3{}^\mu = m^{*\mu}$ .

After these choices, there is still the issue of the normalization of the products  $l^\mu k_\mu$ , and  $m^\mu m^*{}_\mu$ . The rest of the products are zero by construction. All the properties mentioned above can be expressed in the following equations:

$$Z_a{}^\mu Z_{b\mu} = \eta_{ab}, \quad g_{\mu\nu} = 2\eta^{ab} Z_{a(\mu} Z_{b\nu)}, \quad (1)$$

with  $\eta_{ab}$  a matrix of the form

$$\eta_{ab} = \begin{pmatrix} 0 & \eta_{12} & 0 & 0 \\ \eta_{12} & 0 & 0 & 0 \\ 0 & 0 & 0 & -\eta_{12} \\ 0 & 0 & -\eta_{12} & 0 \end{pmatrix}, \quad (2)$$

with  $\eta_{12}$  a constant that depends on the signature. If we choose the signature of the spacetime to be  $(+, -, -, -)$  as in [35, 36], then the choice consistent with Eqs. (1) to derive the perturbation equation is  $\eta_{12} = 1$  [29]. If the spacetime is described using the signature  $(-, +, +, +)$  we have to choose  $\eta_{12} = -1$  in order to remain consistent with Eqs. (1). Some discussion on the change of the tetrad due to the signature can be found in [37].

We derived the perturbation equation for the perturbed Weyl scalar  $\Psi_4$  (note that the background value vanishes), leaving unspecified the choice of signature. Using the definitions for the directional operators and spinor coefficients as given in [35, 36], the final perturbation equation takes the form

$$\begin{aligned} & ((\mathbf{\Delta} + \eta_{12} (4\mu_s + \mu_s^* + 3\gamma_s - \gamma_s^*)) (\mathbf{D} - \eta_{12} (\rho_s - 4\epsilon_s)) - (\delta^* + \eta_{12} (3\alpha_s + \beta_s^* + 4\pi_s - \tau_s^*)) (\delta + \eta_{12} (4\beta_s - \tau_s)) \\ & - 3\eta_{12} \Psi_2) \Psi_4 = 0 \end{aligned} \quad (3)$$

We have added a subindex  $_s$  to the spinor coefficients in order to avoid confusion with other quantities that will be used later. In the rest of the work we will be using the  $(-, +, +, +)$  signature, and thus  $\eta_{12} = -1$ .

### A. Spherical symmetry

We will work in spherically symmetric static spacetimes, and the corresponding metric can be written as

$$g = (-\alpha^2 + \gamma^2 \beta^2) dt^2 + 2\gamma^2 \beta dt dr + \gamma^2 dr^2 + r^2 d\sigma^2. \quad (4)$$

We will write the Bardeen-Press equation for  $\Psi_4$  on such a background with respect to an orthonormal null tetrad  $(l, k, m, \bar{m})$ , consistent with the conditions mentioned above. The tetrad can be given by

$$l^\mu = \frac{1}{2\alpha^2} \left( 1, \frac{\alpha}{\gamma} - \beta, 0, 0 \right), \quad k^\mu = \left( 1, -\left( \frac{\alpha}{\gamma} + \beta \right), 0, 0 \right), \quad m^\mu = \frac{1}{\sqrt{2}r} (0, 0, 1, i \csc \theta), \quad \bar{m}^\mu = (m^\mu)^*.$$

Remember that  $\Psi_4$  is defined by contracting the Weyl tensor with respect to the inward pointing null vector field of the null tetrad,  $k$  in our case.

We compute the corresponding spinor coefficients and directional derivatives and substitute into the general perturbation equation (3). Using the definitions for the spinor coefficients given in [35], and denoting derivatives with respect to  $r$  by a prime, we obtain the non zero spinors and Weyl scalars as

$$\begin{aligned} \rho_s &= \frac{\frac{\alpha}{\gamma} - \beta}{2r\alpha^2}; & \mu_s &= \frac{\frac{\alpha}{\gamma} + \beta}{r}; & \epsilon_s &= -\frac{(r\alpha\gamma\rho_s)'}{2\alpha\gamma}; & \gamma_s &= -\frac{(r\alpha\gamma\mu_s)'}{2\alpha\gamma}; \\ \beta_s &= -\frac{\cot\theta}{2\sqrt{2}r}; & \alpha_s &= -\beta_s, & \Psi_2 &= \frac{(r^2\alpha\gamma\rho_s\mu_s)'}{r\alpha\gamma}. \end{aligned} \quad (5)$$

Before proceeding to write down the perturbation equation for  $\Psi_4$ , we first note that the simple sourceless wave equation,

$$g^{\mu\nu} \nabla_\mu \nabla_\nu \Phi(x^\alpha) = 0, \quad (6)$$

independently of the tensorial or spinorial character of  $\Phi$  in this background takes the general form

$$[\mathcal{O}_{rt} + \mathcal{O}_{\theta\varphi}] \Phi = 0,$$

with

$$\mathcal{O}_{rt} = \frac{r^2}{\alpha^2} \left( -\frac{\partial^2}{\partial t^2} + 2\beta \frac{\partial^2}{\partial t \partial r} + \left( \left( \frac{\alpha}{\gamma} \right)^2 - \beta^2 \right) \frac{\partial^2}{\partial r^2} + \frac{\alpha}{r^2\gamma} \left( \frac{r^2\beta\gamma}{\alpha} \right)' \frac{\partial}{\partial t} + \frac{\alpha}{r^2\gamma} \left( r^2 \left( \frac{\alpha}{\gamma} - \frac{\beta^2\gamma}{\alpha} \right) \right)' \frac{\partial}{\partial r} \right), \quad (7)$$

$$\mathcal{O}_{\theta\varphi} = \frac{\partial^2}{\partial \theta^2} + \frac{1}{\sin^2 \theta} \frac{\partial^2}{\partial \varphi^2} + \cot \theta \frac{\partial}{\partial \theta}. \quad (8)$$

In the perturbation equation (3) we use the sign consistent with our choice of signature, that is  $\eta_{12} = -1$ . After substituting our tetrad and the obtained directional operators, spinor coefficients and the Weyl scalar  $\Psi_2$ , we obtain

$$[L_{tr} + L_{\theta\varphi}] \Psi_4 = 0, \quad (9)$$

where the operators  $L_{tr}$  and  $L_{\theta\varphi}$  are given by

$$L_{tr} = -\frac{r^2}{\alpha^2} \frac{\partial^2}{\partial t^2} + 2\beta \frac{r^2}{\alpha^2} \frac{\partial^2}{\partial t \partial r} + r^2 \left( \frac{\alpha^2 - \beta^2 \gamma^2}{\alpha^2 \gamma^2} \right) \frac{\partial^2}{\partial r^2} + A \frac{\partial}{\partial t} + B \frac{\partial}{\partial r} - 2r^2 C, \quad (10)$$

$$L_{\theta\varphi} = \mathcal{O}_{\theta\varphi} - 4i \frac{\cos \theta}{\sin^2 \theta} \frac{\partial}{\partial \varphi} - 2 \frac{\cos^2 \theta + 1}{\sin^2 \theta}. \quad (11)$$

Here we have defined

$$\begin{aligned} A &= \frac{1}{\alpha \gamma} \left( \frac{r^2 \beta \gamma}{\alpha} \right)' - 4 \frac{r^4 \mu_s}{\alpha^3} \left( \frac{\alpha}{r} \right)', \\ B &= \frac{2}{\alpha \gamma} (r^4 \alpha \gamma \rho_s \mu_s)' - 4r^2 \left( \frac{1}{\gamma^2} \left( \frac{\beta \gamma}{\alpha} \right)' + 2r^3 \frac{\rho_s \mu_s}{\alpha} \left( \frac{\alpha}{r} \right)' \right), \\ C &= \frac{1}{r \alpha \gamma} \left( 3 (\alpha \gamma \rho_s \mu_s r^2)' + \rho_s r (\alpha \gamma \mu_s r)' - 10 \mu_s r (\alpha \gamma \rho_s r)' \right) - \mu_s \left( 5 \rho_s + r \rho_s' + 2r \left( \frac{\alpha \gamma \rho_s r}{\alpha \gamma} \right)' \right) \\ &\quad + \frac{2}{\alpha^2 \gamma^2} (\alpha \gamma \rho_s r)' (\alpha \gamma \mu_s r)', \end{aligned} \quad (12)$$

in terms of the spinor coefficients given in (5).

There are several things worth noticing in this last equation. As expected for a gravitational wave, the principal part is the same as of the wave equation; the actual gravitational contribution is described by some extra coefficients in the terms containing no higher than first radial derivatives. The left hand side of the equation for the gravitational perturbation, as well as that for the wave equation, is separable into terms involving the  $(r, t)$  and the angular coordinates. The equation is somewhat lengthy, due to the fact that we are considering general metric coefficients, but nevertheless, it is quite tractable. Finally, we remark the fact that had we not considered the corresponding change in signature, we would have obtained an inconsistent expression.

We will work with the function  $\tilde{\Psi}_4 = r \Psi_4$ , in order to factor out the expected decay due to the peeling behavior. The function  $\tilde{\Psi}_4$  satisfies the equation:

$$[\tilde{L}_{tr} + L_{\theta\varphi}] \tilde{\Psi}_4 = 0, \quad (13)$$

where the operator  $\tilde{L}_{tr}$  reads

$$\tilde{L}_{tr} = -\frac{r^2}{\alpha^2} \frac{\partial^2}{\partial t^2} + 2\beta \frac{r^2}{\alpha^2} \frac{\partial^2}{\partial t \partial r} + 2r^4 \rho_s \mu_s \frac{\partial^2}{\partial r^2} + \tilde{A} \frac{\partial}{\partial t} + \tilde{B} \frac{\partial}{\partial r} - 2r^2 \tilde{C}, \quad (14)$$

where now

$$\tilde{A} = A - 2r \frac{\beta}{\alpha^2}, \quad \tilde{B} = B - 4r^3 \rho_s \mu_s, \quad \tilde{C} = C + \frac{B}{2r^3} - 2\rho_s \mu_s, \quad (15)$$

and  $A, B$ , and  $C$  are given by (12). Further, using the fact that the Weyl scalar has spin weight  $-2$  [35], we expand  $\tilde{\Psi}_4$  in terms of spin-weighted spherical harmonics:

$$\tilde{\Psi}_4 = \sum_{lm} \phi_{l,m}(t, r) Y_{-2}^{l,m}(\theta, \varphi). \quad (16)$$

To deal with spin-weighted harmonics, it is useful to introduce the so called ‘‘eth’’ and ‘‘eth-bar’’ operators [39, 40]:

$$\bar{\delta}_s = - \left( \frac{\partial}{\partial \theta} + i \csc \theta \frac{\partial}{\partial \varphi} - s \cot \theta \right) \equiv \bar{\delta}_0 + s \cot \theta, \quad (17)$$

$$\delta_s = - \left( \frac{\partial}{\partial \theta} - i \csc \theta \frac{\partial}{\partial \varphi} + s \cot \theta \right) \equiv \delta_0 - s \cot \theta, \quad (18)$$

which have the property of raising and lowering the spin weight of the function on which they act. It is straightforward to show that the angular operator in (11) can be expressed in terms of the eth operators as

$$L_{\theta\varphi} = \bar{\delta}_{-1} \delta_{-2}. \quad (19)$$

The  $Y_{-2}^{l,m}$  are the eigenfunctions of this angular operator:

$$L_{\theta\varphi} Y_{-2}^{l,m} = \bar{\delta}_{-1} \delta_{-2} Y_{-2}^{l,m} = -(l-1)(l+2) Y_{-2}^{l,m}. \quad (20)$$

In this way, the perturbation equation (13) transforms into a 1+1 equation for each  $(l, m)$ -mode of the gravitational perturbation,

$$\left[ \tilde{L}_{tr} - (l-1)(l+2) \right] \phi = 0, \quad (21)$$

where we have dropped the indices  $l, m$ .

### III. INCLUDING NULL INFINITY IN THE NUMERICAL DOMAIN

In the previous section we followed the standard procedure to calculate gravitational perturbations on a spherically symmetric background spacetime using the Teukolsky formalism with the additional feature that we allowed an arbitrary spherically symmetric foliation of the Schwarzschild background (see [38] for the corresponding generalization in the Regge-Wheeler-Zerilli formalism). If we now insert the standard Schwarzschild gauge functions into equation (21) we get the familiar Bardeen-Press equation. Our aim, however, is to include null infinity in the numerical domain. We now show how this can be done.

#### A. Choice of a hyperboloidal foliation

To include null infinity in a 3+1 setting we first choose a hyperboloidal foliation by introducing a new time coordinate,  $\tau$ , whose level sets are hyperboloidal surfaces. Following [28], we consider the class of spherically symmetric constant mean curvature (CMC) foliations of Schwarzschild spacetime [41, 42]. The transformation from the standard Schwarzschild time coordinate to the time coordinate of a spherically symmetric CMC-foliation can be written as  $\tau = t - h(r)$ , where  $r$  is the Schwarzschild area radius,  $h(r)$  is the height function and  $t$  is the standard Schwarzschild time coordinate. The height function is not known in closed form. Its radial derivative is given by

$$h'(r) = \frac{J(r)}{\left(1 - \frac{2m}{r}\right) P(r)}, \quad \text{where} \quad J(r) = \frac{Kr}{3} - \frac{c}{r^2}, \quad \text{and} \quad P(r) := \sqrt{J(r)^2 + \left(1 - \frac{2m}{r}\right)}. \quad (22)$$

Here, the mass of the Schwarzschild black hole is denoted by  $m$ . The foliation parameters are the mean extrinsic curvature  $K$ , and a constant of integration  $c$ . The global behavior of CMC-surfaces depends on the foliation parameters. We choose these parameters such that the surfaces of the foliation come from future null infinity, pass the event horizon above the bifurcation sphere and run into the future singularity as depicted in Figure 1 [43]. The causal nature of our hyperboloidal foliation shown in the conformal diagram explains why we do not need a two stage calculation of the waveform in contrast to the characteristic case [14, 15]. A further convenient feature of our foliation is that our coordinates are adapted to time symmetry in the sense that the timelike Killing vector field of Schwarzschild spacetime  $\partial_t$  is given by  $\partial_\tau$  in the new coordinates. Therefore, timelike curves with constant spatial coordinates can be regarded as worldlines of natural observers at constant distances.

In coordinates adapted to the CMC slicing, the standard Schwarzschild metric is obtained in the form

$$g = - \left(1 - \frac{2m}{r}\right) d\tau^2 - \frac{2J(r)}{P(r)} d\tau dr + \frac{1}{P^2(r)} dr^2 + r^2 d\sigma^2,$$

By comparing with (4) we see that the gauge functions read

$$\alpha(r) = P(r), \quad \beta(r) = -J(r) \alpha(r), \quad \gamma(r) = \frac{1}{\alpha(r)}. \quad (23)$$

An important difference to Cauchy foliations should be noted at this point. The asymptotic behaviour of an asymptotically flat spacetime written in a Cauchy foliation implies  $\alpha \sim 1$  and  $\beta \sim 0$  as  $r \rightarrow \infty$ . The same spacetime written in a hyperboloidal foliation implies a different asymptotic behaviour for the gauge functions, namely

$$\alpha \sim O(r) \quad \text{and} \quad \beta \sim O(r^2) \quad \text{as} \quad r \rightarrow \infty. \quad (24)$$

In the next subsection, we will see that this behaviour is important for the regularity of our equations.

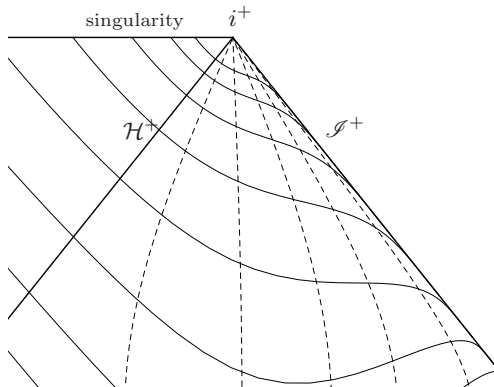


Figure 1: Penrose diagram of a CMC-foliation in Schwarzschild spacetime with  $m = 1/2$ ,  $c = 1$ ,  $K = 1$ . The dashed lines represent Killing observers.

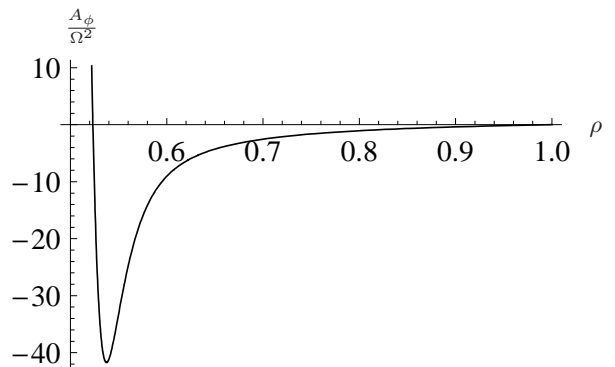


Figure 2: The function  $A_\phi/\Omega^2$  from (28) for the same hyperboloidal foliation as in the diagram. We see that  $C/\Omega^2$  vanishes at null infinity.

## B. Compactification

To include the asymptotic ends of the surfaces of our hyperboloidal foliation, we introduce a compactifying coordinate  $\rho$  that is related to the standard Schwarzschild area-radius  $r$  via

$$r = \frac{\rho}{1-\rho} = \frac{\rho}{\Omega} \quad \text{where} \quad \Omega := 1 - \rho. \quad (25)$$

We choose the black-hole mass as  $m = 1/2$ , the horizon is thus located at  $\rho = 1/2$ . Future null infinity,  $\mathcal{I}^+$ , is located at  $\rho = 1$ . Other choices are, of course, possible. Before writing the Bardeen-Press equation in the compactifying coordinate  $\rho$ , we factor out the singular asymptotic behaviour of our hyperboloidal gauge functions (24) in order to deal with regular functions. Considering the asymptotic behaviour of the conformal factor,  $\Omega \sim 1/r$ , we define  $\bar{\alpha} := \Omega \alpha$  and  $\bar{\beta} := \Omega^2 \beta$ . The rescaled gauge source functions from the previous subsection become

$$\bar{\alpha} = \sqrt{\bar{J}^2 + \left(1 - \frac{2m\Omega}{\rho}\right) \Omega^2}, \quad \bar{\beta} = -\bar{J} \bar{\alpha} \quad \text{where} \quad \bar{J} := \Omega J = \frac{K\rho}{3} - \frac{c\Omega^3}{\rho^2}. \quad (26)$$

These functions are obviously regular at  $\{\Omega = 0\}$ . Furthermore, they satisfy

$$\left(\bar{\alpha}^2 - \frac{\bar{\beta}^2}{\bar{\alpha}^2}\right) = O(\Omega^2) \quad \text{with} \quad \beta|_{\mathcal{I}^+} < 0. \quad (27)$$

We note that this behaviour is specific to the choice of a scri-fixing gauge and cannot be expected for all hyperboloidal foliations. It is related to the fact that the normal to level sets of  $\tau$  lies in  $\mathcal{I}^+$  [43].

The definitions of the auxiliary variables given in (A.1) imply

$$\psi = \partial_r \phi = \Omega^2 \partial_\rho \phi =: \Omega^2 \bar{\psi}, \quad \text{and} \quad \pi = \frac{1}{\alpha^2} (\partial_t \phi - \beta \partial_r \phi) = \frac{\Omega^2}{\bar{\alpha}^2} (\partial_t \phi - \bar{\beta} \bar{\psi}) =: \Omega^2 \bar{\pi}.$$

We write the system (A.2) with respect to the functions  $\bar{\alpha}, \bar{\beta}, \bar{\psi}, \bar{\pi}$  by factoring an  $\Omega^2$  term out of the equations. The resulting first order symmetric hyperbolic system of equations reads

$$\begin{aligned} \partial_\tau \phi &= \bar{\alpha}^2 \bar{\pi} + \bar{\beta} \bar{\psi}, \\ \partial_\tau \bar{\psi} &= \partial_\rho (\bar{\alpha}^2 \bar{\pi} + \bar{\beta} \bar{\psi}), \\ \partial_\tau \bar{\pi} &= \partial_\rho (\bar{\alpha}^2 \bar{\psi} + \bar{\beta} \bar{\pi}) + A_\pi \bar{\pi} + A_\psi \bar{\psi} + \left(\frac{A_\phi}{\Omega^2} - \frac{\lambda}{\rho^2}\right) \phi. \end{aligned}$$

where  $A_\pi, A_\psi$ , and  $A_\phi$  are functions of  $\rho$ . It turns out that  $A_\pi$  and  $A_\psi$  are conformally covariant. Writing  $A_\pi$  and  $A_\psi$  from (A.3) in terms of the rescaled gauge functions and the compactifying coordinate  $\rho$  results in

$$A_\pi = -4(\bar{\alpha}^2 + \bar{\beta}) \partial_\rho \left( \ln \frac{\bar{\alpha}}{\rho} \right), \quad A_\psi = A_\pi - 4\bar{\alpha}^2 \partial_\rho \left( \frac{\bar{\beta}}{\bar{\alpha}^2} \right).$$

To show the regularity of our equations, we need to show that  $A_\phi$  falls off with  $\Omega^2$ . We have by (A.3)

$$\begin{aligned} \frac{A_\phi}{\Omega^2} &= -\frac{\Omega}{\rho} \partial_\rho \left( \frac{1}{\Omega^2} \left( \bar{\alpha}^2 - \frac{\bar{\beta}^2}{\bar{\alpha}^2} \right) \right) + \frac{4}{\Omega \rho} \left( \bar{\alpha}^2 \partial_\rho \left( \frac{\bar{\beta}}{\bar{\alpha}^2} \right) + \left( \bar{\alpha}^2 - \frac{\bar{\beta}^2}{\bar{\alpha}^2} \right) \partial_\rho \left( \ln \frac{\bar{\alpha}}{\rho} \right) \right) \\ &+ 2 \frac{(\bar{\alpha}^2 + \bar{\beta})^2}{\Omega^2 \rho^2} \partial_\rho \left( \frac{\Omega^4 \partial_\rho \left( \frac{\rho^2}{\Omega^2} \left( 1 - \frac{\bar{\beta}}{\bar{\alpha}^2} \right) \right)}{\bar{\alpha}^2 + \bar{\beta}} \right). \end{aligned} \quad (28)$$

The explicit regularity of the above expression follows from the behaviour of our rescaled gauge functions (27), specifically from  $\bar{\alpha}^2 + \bar{\beta} \sim O(\Omega^2)$  near null infinity. Indeed, as we can see in Figure 2 the expression on the right hand side of (28) is not just regular but vanishes at null infinity for the foliation given in (26). We note that scri-fixing plays an essential role here.

## IV. NUMERICAL STUDIES

### A. Initial data

As we are not interested in the first (transient) part of the signal, the initial data can be chosen quite freely. We take a simple Gaussian as the initial perturbation and set

$$\phi(0, \rho) = a e^{-(\rho - \rho_c)^2 / \sigma^2}, \quad \psi(0, \rho) = \partial_\rho \phi(0, \rho), \quad \pi(0, \rho) = 0.$$

Here,  $\rho_c$  is the center of the Gaussian pulse,  $a$  is its amplitude and  $\sigma$  is its width. We set  $\rho_c = 0.7, a = 1$  and  $\sigma = 0.05$  on the domain  $\rho \in [0.495, 1]$  in the numerical calculations. The solid line in Figure 7 shows the initial data. We have tested that different choices of initial data do not have a relevant influence on the features we discuss in the following. Note that the vanishing of  $\pi(0, r)$  does not mean that the data is time symmetric, because the initial surface is future hyperboloidal (spacelike while approaching future null infinity). We focus on the typically dominant  $l = 2$  mode, corresponding to the lowest allowed angular momentum number for a spin-2 field because higher modes are weaker due to their faster decay rates and longer quasinormal mode ringing phases.

### B. Numerical algorithms

We adopt the method of lines approach and discretize time and space separately, using 4th order Runge-Kutta time integration and finite differencing with 4th, 6th and 8th order accurate stencils. We add Kreiss-Oliger type artificial dissipation to the evolution equation for  $\pi$  to suppress high-frequency waves [44]. For a  $2p - 2$  accurate scheme we choose an operator ( $Q$ ) of order  $2p$  as

$$Q = \epsilon (-1)^p \frac{h^{2p-1}}{2^p} D_+^p D_-^p,$$

where  $h$  is the grid size,  $D_\pm$  are the forward and backward finite differencing operators and  $\epsilon$  is our dissipation parameter. Unless otherwise stated, we set  $\epsilon = 0.07$ .

The inner boundary is a spacelike surface inside the event horizon where no boundary data is required. We excise the interior domain near the singularity. For the class of CMC surfaces we have chosen, excision is necessary as there is a minimal surface inside the event horizon where our coordinates break down. The outer boundary is at null infinity where one-sided finite differencing is applied. The one-sided finite differencing is of the same order as the interior one.

The convergence of the code can be seen in Figure 3. For this plot, a three level convergence analysis has been performed with 505, 1010 and 2020 grid cells using finite difference operators of 4th, 6th and 8th order. For the 6th and 8th order convergence tests, we used quadruple precision because the numerical error was below machine accuracy at late times when double precision was used. At very late times, convergence is lost due to accumulation of numerical errors (see the bending down of the curves in Figure 9 at late times).

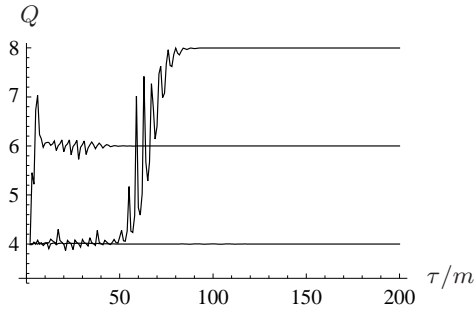


Figure 3: Convergence in the L2-norm indicating 4th, 6th and 8th order convergence for the corresponding finite difference operators. The convergence factor  $Q$  is calculated by  $Q = \log_2 \frac{\|\phi^{low} - \phi^{med}\|}{\|\phi^{med} - \phi^{high}\|}$ .

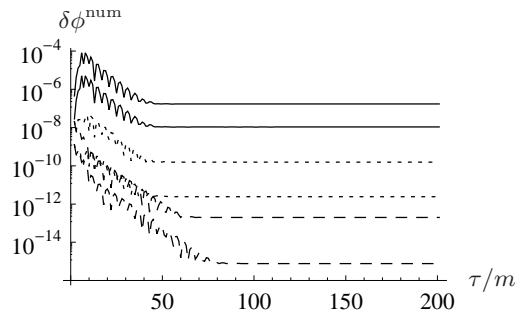


Figure 4: L2-norm of the differences between numerical solutions obtained using different resolutions, i.e.  $\|\phi^{low} - \phi^{med}\|$  and  $\|\phi^{med} - \phi^{high}\|$ . Solid curves denote errors for 4th order finite difference operators, pointed curves for 6th order and dashed curves for 8th order.

Figure 4 shows the L2-norm of the relative errors between the above mentioned simulations in different resolutions and finite differencing orders. We observe that using an 8th order accurate finite differencing improves the final error by 8 orders of magnitude in the high resolution runs. The numerical error in the high resolution run is smaller than machine accuracy when double precision is used. We see that high accuracies can be achieved using high order finite differencing in combination with a relatively small amount of grid points.

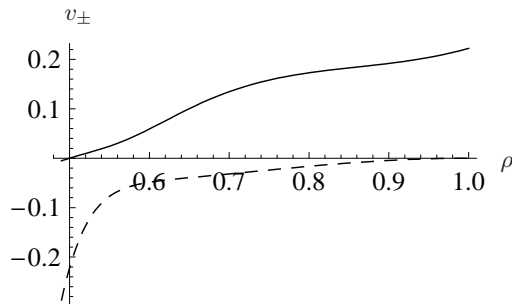


Figure 5: The dashed and the solid curves denote coordinate speeds of in- and outgoing characteristics respectively, for the foliation characterized by (26). The horizon is located at  $\rho = 0.5$ . We see that the characteristic speeds are less than unity which allows us to choose a large Courant factor. We observe that there is little variation of the speeds over the grid which has infinite physical extent.

The simulation domain in the compactifying coordinate reads  $\rho \in [0.495, 1]$ . The Courant factor  $\Delta t/\Delta\rho$  in the simulations has been chosen to be 4. We can choose a Courant factor that is larger than 1 because the coordinate speeds of characteristics are less than 1. For outgoing and ingoing characteristics, the characteristic speeds with respect to our foliation are  $v_{\pm} = \pm\bar{\alpha}^2 - \bar{\beta}$ . Figure 5 shows the characteristic speeds along the grid. The allowed Courant factor depends on the value of  $K$  as  $K$  is related to the coordinate speed of characteristics. For example, the coordinate speed of outgoing characteristics at  $\mathcal{S}^+$  reads in our foliation  $v_+|_{\mathcal{S}^+} = 2K^2/9$ . Therefore, a large value for  $K$  implies a small Courant factor [43]. We plot in Figure 5 the speeds for  $K = 1$  and see that  $v_{\pm} < 1$  which allows  $\Delta t/\Delta\rho > 1$ . We also see that the ingoing characteristic speed vanishes at  $\mathcal{S}^+$  as expected, correspondingly we do not need to impose outer boundary conditions. Note also that there is relatively little variation of the characteristic speeds over this grid which has infinite physical extent.

In the studies presented below, we choose  $m = 1/2$ ,  $c = 1$  and  $K = 1$ .

### C. Quasinormal mode ringing

Figure 6 shows the gravitational perturbations of a Schwarzschild black hole in a double logarithmic plot with respect to three observers located at  $r \approx \{2.5m, 18m\}$  and at  $\mathcal{S}^+$ . We see that, as expected, the quasinormal mode frequencies are the same for these observers. It does not matter for the calculation of these frequencies at what distance from the black hole the perturbations are measured. We see, however, that the end of the quasinormal

ringing phase is observer-dependent. The polynomially decaying part of the solution starts earlier for an observer at  $\mathcal{I}^+$  than for a nearby observer. This suggests that for the calculation of quasi-normal mode frequencies, one may get better results by using the waveform as measured by a nearby observer.

We expect the quasinormal mode ringing to have the form

$$\phi_\rho(\tau) = a_\rho e^{-\omega_2 \tau} \sin(\omega_1 \tau + \varphi_\rho). \quad (29)$$

Here,  $\omega_1$  and  $\omega_2$  are the mode frequencies,  $a_\rho$  is the amplitude and  $\phi_\rho$  is the phase of the wave signal. In contrast to the mode frequencies, the amplitude and the phase do depend in general on the observer's location.

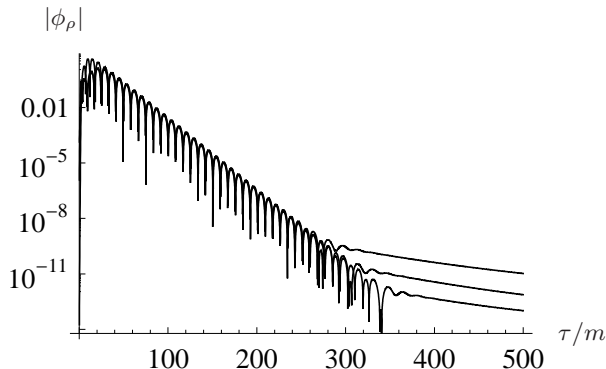


Figure 6: Quasi normal mode ringing of Schwarzschild spacetime excited by a Gaussian gravitational perturbation with  $l = 2$  measured by three observers. Looking to the tail part of the signal, the observers are located from top to bottom at  $\mathcal{I}^+$ ,  $r \approx 18m$  and  $r \approx 2.5m$ . We see that the ringing phase ends at different times for different observers and goes into a polynomial decay.

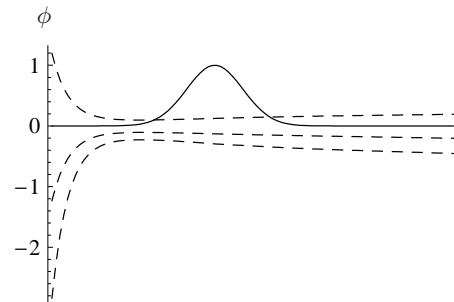


Figure 7: The numerical solution on the grid during the quasinormal ringing phase plotted at different times and rescaled for visibility. The solid curve is just the initial data. The dashed curves are from top to bottom:  $\{10 \times \phi(80m, \rho), 100 \times \phi(106m, \rho), 1000 \times \phi(122m, \rho)\}$ . We see that the wave package is distributed quite uniformly across the grid.

To demonstrate the efficiency of our method, we calculate the quasinormal mode frequencies during the ringing phase using various resolutions. The frequencies are compared to the result from Leaver's continued fraction method [45]. For our choice of black hole mass of  $m = 1/2$  they read  $(\omega_1, \omega_2) = (0.747343, 0.177925)$ . Table I shows the measured frequencies for various grid resolutions for 4th and 6th order finite differencing operators along with the relative errors. The relative error  $\delta\omega_i^{(2p)}$  for  $\omega_i^{\text{num}(2p)}$  in a numerical simulation with spatial finite differencing of order  $2p$  is calculated by  $\delta\omega_i^{(2p)} = |\omega_i^{\text{num}(2p)} - \omega_i|/\omega_i$ . The fitting is performed using a simple least squares method on the interval  $\tau \in [80m, 180m]$  with an initial guess of the frequencies.

Cells	$\omega_1^{\text{num}(4)}$	$\omega_2^{\text{num}(4)}$	$\delta\omega_1^{(4)}$	$\delta\omega_2^{(4)}$	$\omega_1^{\text{num}(6)}$	$\omega_2^{\text{num}(6)}$	$\delta\omega_1^{(6)}$	$\delta\omega_2^{(6)}$
25 <sup>a</sup>	0.825455	0.157916	$10^{-2}$	$1.1 \times 10^{-2}$	0.777778	0.168439	$4.1 \times 10^{-2}$	$5.3 \times 10^{-2}$
50	0.746988	0.177897	$4.7 \times 10^{-4}$	$1.5 \times 10^{-4}$	0.747341	0.177917	$2.3 \times 10^{-6}$	$4.4 \times 10^{-5}$
100	0.747325	0.177927	$2.4 \times 10^{-5}$	$1.1 \times 10^{-5}$	0.747344	0.177923	$1.9 \times 10^{-6}$	$9.5 \times 10^{-6}$
200	0.747343	0.177924	$2.6 \times 10^{-7}$	$4.9 \times 10^{-6}$	0.747344	0.177924	$1.8 \times 10^{-6}$	$5.4 \times 10^{-6}$

<sup>a</sup>For the runs with 25 grid cells, a relatively high dissipation parameter of  $\epsilon = 0.2$  has been used.

TABLE I: Numerical quasinormal mode frequencies  $\omega_i^{\text{num}(2p)}$  in various resolutions measured at  $r \approx 2.5m$  and the relative errors  $\delta\omega_i^{(2p)}$  calculated in a numerical simulation with spatial finite difference operators of the order  $2p$ . We perform a simple least square fit to (29) with initial guess. We see that even with low resolutions, we are able to measure the quasinormal-mode frequencies with a high accuracy indicating the efficiency of our method.

We see that already with 50 cells we are able to calculate the quasinormal mode frequencies with a relative error of about  $10^{-4}$  using 4th order finite differences and  $10^{-6}$  using 6th order finite differences. The use of higher order accurate finite differencing does not increase the computational cost significantly. We observed only about a 5% increase in the run time for the 6th order finite differencing compared to the 4th order one. We note that for a relative error at the order of  $10^{-6}$ , the accuracy in the frequency is rather dominated by the fit than by numerics. This explains, in part, why the relative error in the simulation with 200 grid cells seems smaller in the 4th order case

than in the 6th order case. Using 8th order finite differencing gives similar results as the 6th order one and does not increase the accuracy in the frequencies considerably.

The fact that using a very small number of cells is already sufficient for such accuracy in the frequencies demonstrates the efficiency of the hyperboloidal approach. An explanation for this efficiency can be found in the way the solution looks like. Figure 7 shows the solution at three different times during the quasinormal ringing phase. We see that the initially localized perturbation is distributed uniformly on the grid. This uniform distribution implies that there is no need to use a high number of grid points to resolve the outgoing wave package. For accuracy, it is more efficient to use a high order scheme with a small number of grid points in this case. In evolutions with Cauchy-type foliations, however, the outgoing wave package is a long wave-train with the typical quasinormal ringing form that requires good resolution. We note that the observed broadening in the hyperboloidal approach is stronger for larger values of  $K$ . For smaller values we get a similar localization like when Cauchy-type foliations are used. This is because  $K$  can be regarded as a measure of how close the behaviour of hyperboloidal surfaces is to being characteristic [43].

#### D. Polynomial decay

Figure 8 shows the polynomially decaying part of the solution starting from  $\tau = 500m$  as seen at future null infinity,  $\mathcal{I}^+$ , at  $r \approx 60m$  and at the future horizon,  $\mathcal{H}^+$ , in an evolution with 4040 grid cells. We observe that the scattered perturbations are stronger for the observer at  $\mathcal{I}^+$  and also the slope of the curves are different, indicating that the decay rate for a far away observer is less than the decay rate for a close by observer. An intuitive explanation for this difference is given by the picture that the tail is generated by backscattering off the nonvanishing curvature of the background spacetime. An observer who is farther away sees more scattering than a nearby observer. Therefore, the amount of scattered waves measured by a nearby observer is less than for a farther one, consequently the scattered part of the signal is “stronger” for the far away observer (modulo the natural fall-off) and decays slower. The natural fall-off is not seen in Figure 8 as the variable we plot is the real part of  $\Psi_4$  rescaled with  $r$ .

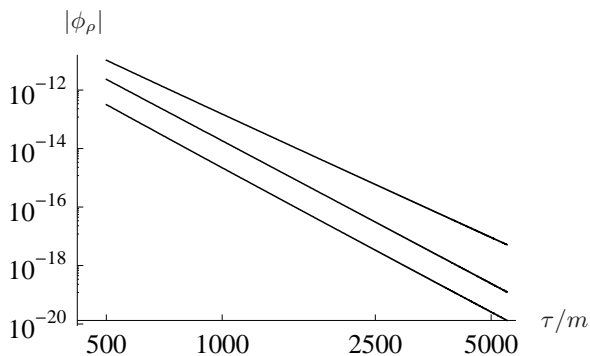


Figure 8: The polynomially decaying part of the solution in a double-logarithmic plot starting from  $\tau = 500m$ . The upper curve gives the solution at null infinity, the middle one at  $r \approx 60m$  and the lower one at the future horizon  $\mathcal{H}^+$ . It can be seen that the decay of the solution along  $\mathcal{I}^+$  is slower than near the black hole.

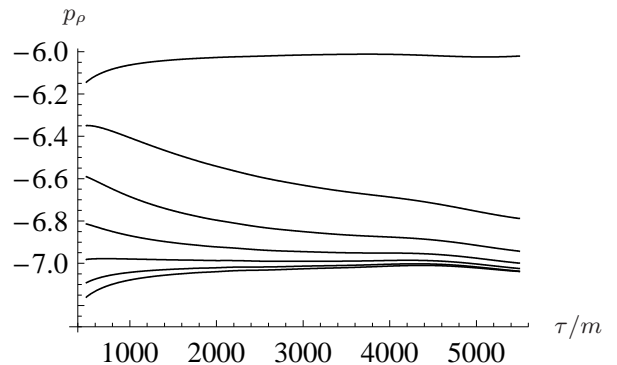


Figure 9: The local power index  $p_\rho(\tau)$  for observers located from top to bottom at  $\{\mathcal{I}^+, 800m, 260m, 110m, 50m, 25m\}$ . We see that after about  $\tau = 4500m$  the local power index for nearby observers bends down. This behaviour is seen earlier for lower resolutions and is only a numerical effect indicating loss of convergence due to loss of accuracy.

We see from Figures 6 and 8 that we are able to follow the solution for more than 20 orders of magnitude and calculate the predicted decay rate with a high accuracy. To achieve such accuracy, we use 8th order finite difference operators. The exponentially decaying (quasinormal mode ringing) part of the solution is calculated in quadruple precision. The reason for choosing 8th order accurate finite differencing is due to the very small effects that we are trying to measure. Note that for any given finite difference order, there are ghost potentials which may be mistaken as tail solutions [46]. We have tested that the tail seen in Figure 8 is not a numerical artefact by comparing solutions in various resolutions.

An accurate picture of the decay rates can be obtained from Figure 9. Here we plot the local power index for various observers defined as

$$p_\rho(\tau) = \frac{d \ln |\phi(\tau, \rho)|}{d \ln \tau}. \quad (30)$$

The function  $p_\rho(\tau)$  becomes asymptotically the exponent of the polynomial decay of the solution. At late times, our numerically measured decay rate becomes  $-6.01$  for an observer at  $\mathcal{S}^+$  and  $-7.002$  for an observer near  $i^+$ , in accordance with the well-known prediction of  $2^{-(2l+2)}$  at  $\mathcal{S}^+$  and of  $2^{-(2l+3)}$  near  $i^+$  [47] (see also [26, 48–51]).

## V. DISCUSSION

In this paper we have revisited the problem of scattering pulses of gravitational waves off a Schwarzschild black hole with the aim of getting guidance in the development of a hyperboloidal approach to numerical relativity. We have used constant mean curvature slices on the background of a Schwarzschild spacetime [41, 42] in a scri-fixing gauge [43] to numerically solve a hyperboloidal initial value problem [28] for the Bardeen-Press equation. The numerical study of gravitational perturbations at null infinity follows, in some sense, the spirit of [14–16] who studied compactified null foliations.

Motivation for taking a hyperboloidal approach comes from the well-known shortcomings of existing methods based on Cauchy-type and characteristic foliations for this problem. The drawbacks of using Cauchy-type foliations can be summarized as follows: (i) waste of computational resources when one is interested in the waveform as seen by far away observers, (ii) spurious reflections from the outer boundary contaminating the waveform in long time evolutions due to unknown boundary data, (iii) not being able to read off the waveform at null infinity. Using a characteristic foliation solves these problems, but leads to new difficulties: (i) the causal relationship between the surfaces necessitates a two-stage approach [14, 15], (ii) choice of variables for the numerical simulations is not straightforward due to loss of resolution, and most importantly, (iii) extension beyond spherical symmetry is very complicated. Especially in highly dynamical situations where formation of caustics is expected [52], it is not yet clear how the characteristic approach can be implemented [53].

The hyperboloidal approach hopes to combine the best properties of currently used approaches in the field, namely the flexibility of Cauchy-type surfaces and the asymptotic behaviour of characteristic surfaces, and avoids their problems – however it is also much less developed so far.

We believe that the problem of treating gravitational perturbations on a fixed spherically symmetric background, while rather simple, is an important step in the development of algorithms for the hyperboloidal initial value problem. We have chosen to solve the Bardeen-Press equation describing perturbations of Schwarzschild spacetime in terms of the Weyl component  $\psi_4$ , partly because this naturally generalizes to the much more interesting axisymmetric case via the Teukolsky equation.

We demonstrated in this paper that compactification along hyperboloidal surfaces using the Teukolsky formalism on the background of a Schwarzschild spacetime leads to regular equations. This regular behaviour can be expected on the background of any weakly asymptotically simple spacetime (in the sense of Penrose [54, 55]). The resulting equations can be solved numerically to study quasinormal mode ringing very efficiently. The tail part can be calculated accurately with sufficient numerical resolution. There are no reflections from the numerical outer boundary. The only approximation we use to calculate the gravitational waveform besides the linearization is the numerical discretization of the equations. The observed uniform distribution of outgoing wave packages along the grid and the numerical experiments we performed suggest that the use of high order methods to solve the linear perturbation equations lead to an efficient code that requires a moderate number of grid points while achieving high accuracy in the results.

We want to conclude with a brief discussion of open problems for future work. It will be interesting to compare the approach for curvature-based and metric perturbations using the Chandrasekhar transformation along the lines of [11]. Current work is under way to study metric perturbations using the Regge-Wheeler-Zerilli formalism in a hyperboloidal setting [56]. The hyperboloidal approach to study gravitational perturbations at null infinity should generalize rather straightforwardly to Kerr spacetime, for example by using the foliations presented in [43].

The difficulty of generalization to the fully nonlinear Einstein equations remains unclear. In contrast to the test field case, the conformally rescaled Einstein equations are not explicitly regular. There, a scri-fixing gauge can be constructed in a hyperboloidal initial value problem for the generalized harmonic reduction of the Einstein equations such that the formally singular terms attain regular limits at null infinity [57]. The open question is whether such limits can be calculated numerically in a stable way. The asymptotic behaviour of the gauge functions (27) need to be taken into account if a regularization along the lines of [57] needs to be done for the ADM or BSSN systems based on scri-fixing. A very promising alternative is to adopt an elliptic-hyperbolic formulation of the problem, and apply boundary conditions for gauge quantities as an elliptic Dirichlet problem, as suggested in [58].

### Acknowledgments

This work was supported in part by the NSF grant PHY0801213 to the University of Maryland and by the DFG grant SFB/Transregio 7 ‘‘Gravitational Wave Astronomy’’. S. Husa is a VESF fellow of the European Gravitational Observatory (EGO). D Nunez is grateful to Luciano Rezzolla for warm hospitality during his stay at the AEI, and acknowledges DAAD, DGAPA-UNAM and CONACyT grants for partial support.

### Appendix: Symmetric hyperbolic form of the Bardeen-Press equation

We solve the Bardeen-Press equation in first order symmetric hyperbolic form using a spherically symmetric CMC-foliation of Schwarzschild spacetime with the gauge functions given in (23). The relation  $\alpha = 1/\gamma$  simplifies the calculation, so we will assume it in the following. In such a gauge, the spinor coefficients take the form

$$\rho_s = \frac{\alpha^2 - \beta}{2\alpha^2 r}, \quad \mu_s = \frac{\alpha^2 + \beta}{r}.$$

To bring the radial part of the Bardeen-Press equation (21) to first order form, we introduce the auxiliary variables

$$\psi := \partial_r \phi, \quad \text{and} \quad \pi := \frac{1}{\alpha^2} (\partial_t \phi - \beta \partial_r \phi). \quad (\text{A.1})$$

Then the following linear, symmetric hyperbolic system of evolution equations is obtained from (14), (15)

$$\begin{aligned} \partial_t \phi &= \alpha^2 \pi + \beta \psi, \\ \partial_t \psi &= \partial_r (\alpha^2 \pi + \beta \psi), \\ \partial_t \pi &= \partial_r (\alpha^2 \psi + \beta \pi) + A_\pi \pi + A_\psi \psi + \left( A_\phi - \frac{\lambda}{r^2} \right) \phi, \end{aligned} \quad (\text{A.2})$$

with  $\lambda = (l-1)(l+2)$  and

$$\begin{aligned} A_\pi &= -4(\alpha^2 + \beta) \partial_r \left( \ln \frac{\alpha}{r} \right), \\ A_\psi &= A_\pi - 4\alpha^2 \partial_r \left( \frac{\beta}{\alpha^2} \right), \\ A_\phi &= -\frac{1}{r} \partial_r \left( \alpha^2 - \frac{\beta^2}{\alpha^2} \right) + \frac{4}{r} \left( \alpha^2 \partial_r \left( \frac{\beta}{\alpha^2} \right) + \left( \alpha^2 - \frac{\beta^2}{\alpha^2} \right) \partial_r \left( \ln \frac{\alpha}{r} \right) \right) + \frac{2(\alpha^2 + \beta)^2}{r^2} \partial_r \left( \frac{\partial_r \left( r^2 \left( 1 - \frac{\beta}{\alpha^2} \right) \right)}{\alpha^2 + \beta} \right). \end{aligned} \quad (\text{A.3})$$

- 
- [1] Frans Pretorius. Evolution of binary black hole spacetimes. *Phys. Rev. Lett.*, 95:121101, 2005.
  - [2] Manuela Campanelli, C. O. Lousto, P. Marronetti, and Y. Zlochower. Accurate evolutions of orbiting black-hole binaries without excision. *Phys. Rev. Lett.*, 96:111101, 2006.
  - [3] John G. Baker, Joan Centrella, Dae-Il Choi, Michael Koppitz, and James van Meter. Gravitational wave extraction from an inspiraling configuration of merging black holes. *Phys. Rev. Lett.*, 96:111102, 2006.
  - [4] Mark Hannam, Sascha Husa, Bernd Brugmann, and Achamveedu Gopakumar. Comparison between numerical-relativity and post-Newtonian waveforms from spinning binaries: the orbital hang-up case. 2007.
  - [5] Ian Hinder, Frank Herrmann, Pablo Laguna, and Deirdre Shoemaker. Comparisons of eccentric binary black hole simulations with post-Newtonian models. 2008.
  - [6] Manuela Campanelli, Carlos O. Lousto, Hiroyuki Nakano, and Yosef Zlochower. Comparison of Numerical and Post-Newtonian Waveforms for Generic Precessing Black-Hole Binaries. 2008.
  - [7] Michael Boyle et al. High-accuracy numerical simulation of black-hole binaries: Computation of the gravitational-wave energy flux and comparisons with post-Newtonian approximants. 2008.
  - [8] John G. Baker et al. Mergers of non-spinning black-hole binaries: Gravitational radiation characteristics. *Phys. Rev.*, D78:044046, 2008.
  - [9] Mark Hannam, Sascha Husa, Ulrich Sperhake, Bernd Brugmann, and Jose A. Gonzalez. Where post-Newtonian and numerical-relativity waveforms meet. 2007.
  - [10] Michael Boyle et al. High-accuracy comparison of numerical relativity simulations with post-Newtonian expansions. *Phys. Rev.*, D76:124038, 2007.

- [11] Manuela Campanelli, William Krivan, and Carlos O. Lousto. The imposition of Cauchy data to the Teukolsky equation II: Numerical comparison with the Zerilli-Moncrief approach to black hole perturbations. *Phys. Rev.*, D58:024016, 1998.
- [12] John G. Baker, Manuela Campanelli, and Carlos O. Lousto. The Lazarus project: A pragmatic approach to binary black hole evolutions. *Phys. Rev.*, D65:044001, 2002.
- [13] Enrique Pazos-Avalos and Carlos O. Lousto. Numerical integration of the Teukolsky equation in the time domain. *Phys. Rev.*, D72:084022, 2005.
- [14] Sascha Husa, Yosef Zlochower, Roberto Gomez, and Jeffrey Winicour. Retarded radiation from colliding black holes in the close limit. *Phys. Rev.*, D65:084034, 2002.
- [15] Manuela Campanelli, Roberto Gomez, Sascha Husa, Jeffrey Winicour, and Yosef Zlochower. The close limit from a null point of view: The advanced solution. *Phys. Rev.*, D63:124013, 2001.
- [16] Yosef Zlochower, Roberto Gomez, Sascha Husa, Luis Lehner, and Jeffrey Winicour. Mode coupling in the nonlinear response of black holes. *Phys. Rev.*, D68:084014, 2003.
- [17] Piotr Bizon, Tadeusz Chmaj, and Andrzej Rostworowski. On asymptotic stability of the Skyrmion. *Phys. Rev.*, D75:121702, 2007.
- [18] Piotr Bizon, Tadeusz Chmaj, and Andrzej Rostworowski. Late-time tails of a Yang-Mills field on Minkowski and Schwarzschild backgrounds. *Class. Quant. Grav.*, 24:F55, 2007.
- [19] John G. Baker et al. Nonlinear and Perturbative Evolution of Distorted Black Holes. II. Odd-parity Modes. *Phys. Rev.*, D62:127701, 2000.
- [20] John G. Baker, Manuela Campanelli, C. O. Lousto, and R. Takahashi. Modeling gravitational radiation from coalescing binary black holes. *Phys. Rev.*, D65:124012, 2002.
- [21] John G. Baker, Manuela Campanelli, Carlos O. Lousto, and R. Takahashi. Coalescence remnant of spinning binary black holes. *Phys. Rev.*, D69:027505, 2004.
- [22] Manuela Campanelli, Bernard J. Kelly, and Carlos O. Lousto. The Lazarus project II: Space-like extraction with the quasi-Kinnersley tetrad. *Phys. Rev. D*, 73:064005, 2006.
- [23] J. M. Bardeen and W. H. Press. Radiation fields in the Schwarzschild background. *J. Math. Phys.*, 14:7–19, 1973.
- [24] Elspeth W. Allen, Elizabeth Buckmiller, Lior M. Burko, and Richard H. Price. Radiation tails and boundary conditions for black hole evolutions. *Phys. Rev.*, D70:044038, 2004.
- [25] Mihalis Dafermos and Igor Rodnianski. A note on boundary value problems for black hole evolutions. 2004.
- [26] Edward W. Leaver. Spectral decomposition of the perturbation response of the Schwarzschild geometry. *Phys. Rev.*, D34:384–408, 1986.
- [27] Michael Pürrer, Sascha Husa, and Peter C. Aichelburg. News from critical collapse: Bondi mass, tails and quasinormal modes. *Phys. Rev.*, D71:104005, 2005.
- [28] Anil Zenginoğlu. A hyperboloidal study of tail decay rates for scalar and Yang-Mills fields. *Class. Quant. Grav.*, 25:175013, 2008.
- [29] S. A. Teukolsky. Perturbations of a rotating black hole I. Fundamental equations for gravitational, electromagnetic, and neutrino-field perturbations. *Astroph. J.*, 185:635–647, 1973.
- [30] Liebrecht R. Venter and Nigel T. Bishop. Numerical validation of the Kerr metric in Bondi-Sachs form. *Phys. Rev.*, D73:084023, 2006.
- [31] Frans Pretorius and Werner Israel. Quasi-spherical light cones of the Kerr geometry. *Class. Quant. Grav.*, 15:2289–2301, 1998.
- [32] Helmut Friedrich. Cauchy problems for the conformal vacuum field equations in general relativity. *Comm. Math. Phys.*, 91:445–472, 1983.
- [33] Sascha Husa, Carsten Schneemann, Tilman Vogel, and Anil Zenginoglu. Hyperboloidal data and evolution. *AIP Conf. Proc.*, 841:306–313, 2006.
- [34] E. Newman and R. Penrose. An approach to gravitational radiation by a method of spin coefficients. *J. Math. Phys.*, 3:566–579, 1962.
- [35] S. Chandrasekhar. *The mathematical theory of black holes*. Clarendon Press Oxford, Oxford, UK, 1983.
- [36] V. Frolov. Newman-penrose method in the general relativistic theory (in Russian). *Science Academy USSR*, 96:72–180, 1977.
- [37] F. J. Ernst. Coping with different languages in the null tetrad formulation of general relativity. *J. Math. Phys.*, 19:489–493, 1978.
- [38] Olivier Sarbach and Manuel Tiglio. Gauge invariant perturbations of Schwarzschild black holes in horizon-penetrating coordinates. *Phys. Rev.*, D64:084016, 2001.
- [39] E. Newman and R. Penrose. Note on the Bondi-Metzner-Sachs group. *J. Math. Phys.*, 7:863–870, 1966.
- [40] J. N. Goldberg, A. J. Macfarlane, E. Newman, F. Rohrlich, and E. C. G. Sudarshan. Spin s spherical harmonics and eth. *J. Math. Phys.*, 8:2155–2161, 1967.
- [41] Dieter R. Brill, John M. Cavallo, and James A. Isenberg. K-surfaces in the Schwarzschild space-time and the construction of lattice cosmologies. *Journal of Mathematical Physics*, 21(12):2789–2796, 1980.
- [42] Edward Malec and Niall O Murchadha. Constant mean curvature slices in the extended Schwarzschild solution and collapse of the lapse: Part I. *Phys. Rev. D*, 68:124019, 2003.
- [43] Anil Zenginoğlu. Hyperboloidal foliations and scri-fixing. *Class. Quant. Grav.*, 25:145002, 2008.
- [44] H. O. Kreiss and J.. Olinger. *Methods for the approximate solution of time dependent problems*. International Council of Scientific Unions, World Meteorological Organization, Geneva, 1973.
- [45] E. W. Leaver. An analytic representation for the quasi normal modes of Kerr black holes. *Proc. Roy. Soc. Lond.*, A402:285–

- 298, 1985.
- [46] E. S. C. Ching, P. T. Leung, W. M. Suen, and K. Young. Wave propagation in gravitational systems: Late time behavior. *Phys. Rev. D*, 52(4):2118–2132, 1995.
  - [47] R. Price. Nonspherical perturbations of relativistic gravitational collapse. I. Scalar and gravitational perturbations. *Phys. Rev. D*, 5:2419, 1972.
  - [48] C. Gundlach, R. Price, and J. Pullin. Late-time behaviour of stellar collapse and explosions: I. linearized perturbations. *Phys. Rev. D*, 49, 1994.
  - [49] C. Gundlach, R. Price, and J. Pullin. Late-time behaviour of stellar collapse and explosions: II. nonlinear evolution. *Phys. Rev. D*, 49, 1994.
  - [50] Leor Barack. Late time dynamics of scalar perturbations outside black holes. I: A shell toy-model. *Phys. Rev. D*, 59:044016, 1999.
  - [51] Leor Barack. Late time dynamics of scalar perturbations outside black holes. II: Schwarzschild geometry. *Phys. Rev. D*, 59:044017, 1999.
  - [52] Helmut Friedrich and John Stewart. Characteristic initial data and wavefront singularities in general relativity. *Proc. R. Soc.*, A385:345–371, 1983.
  - [53] Jeffrey Winicour. Characteristic evolution and matching. *Living Rev. Relativity*, 8:10, 2005. [Online article].
  - [54] Roger Penrose. Asymptotic properties of fields and space-times. *Phys. Rev. Lett.*, 10:66–68, 1963.
  - [55] Roger Penrose. Zero rest-mass fields including gravitation: Asymptotic behaviour. *Proc. Roy. Soc. Lond.*, A284:159–203, 1965.
  - [56] Vincent Moncrief. Private communication.
  - [57] Anıl Zenginoğlu. Hyperboloidal evolution with the Einstein equations. *Class. Quant. Grav.*, 25:195025, 2008.
  - [58] Lars Andersson. Construction of hyperboloidal initial data. *Lect. Notes Phys.*, 604:183–194, 2002.